MOTION NEAR THE 3/1 RESONANCE OF THE PLANAR ELLIPTIC RESTRICTED THREE BODY PROBLEM

JACQUES HENRARD

Département de mathématique, FUNDP,
Rempart de la Vierge, 8, B-5000 Namur, Belgium

N.D. CARANICOLAS

Department of Astronomy, University of Thessaloniki,
54006 Thessaloniki, Greece

(Received : 11 October 1988; accepted : 17 November 1989)

Abstract. The global semi-numerical perturbation method proposed by Henrard and Lemaître (1986) for the 2/1 resonance of the planar elliptic restricted three body problem is applied to the 3/1 resonance and is compared with Wisdom's perturbative treatment (1985) of the same problem. It appears that the two methods are comparable in their ability to reproduce the results of numerical integration especially in what concerns the shape and area of chaotic domains. As the global semi-numerical perturbation method is easily adapted to more general types of perturbations, it is hoped that it can serve as the basis for the analysis of more refined models of asteroidal motion. We point out in our analysis that Wisdom's uncertainty zone mechanism for generating chaotic domains (also analysed by Escande 1985 under the name of slow Hamiltonian chaotic layer) is not the only one at work in this problem. The secondary resonance $\omega_p = 0$ plays also its role which is qualitatively (if not quantitatively) important as it is closely associated with the random jumps between a high eccentricity mode and a low eccentricity mode.

Keywords: resonance, Kirkwood gaps, perturbation method, chaotic motion, secondary resonance

1. Introduction

The existence of the Kirkwood gaps in the asteroid belt and their unmistakable association with resonances has been a puzzling problem in Celestial Mechanics for a long time; puzzling and important because the peculiarities in the distribution of asteroids could contain some hidden clues on how the Solar System formed or evolved.

The natural satellite systems have also provided a long list of puzzles involving origin and evolution of resonances between satellites (see Peale 1986 for a recent review). Again, the present orbital configurations together with the evidences, recently obtained, of late resurfacing of small icy satellites could contain precious information on the physics of the Solar System.

In both cases, what we need to untangle those clues is a sharp understanding of the long term behaviour of trajectories near commensurability in the elliptic restricted three body problem.

Our understanding of the dynamics of this problem has been much improved (see Henrard 1988 for a review) by the work of Scholl and Froeschlé (1974, 1975),

Celestial Mechanics and Dynamical Astronomy 47: 99–121, 1990.

Froeschlé and Scholl (1976, 1977, 1981) and more recently by the work of Wisdom (1982, 1983, 1985).

In particular, Wisdom (1985) proposed a perturbative treatment of the motion near the 3/1 commensurability by which one could understand, in an unified way, most of the peculiarities found numerically by him and previous authors.

Unfortunately, Wisdom's perturbative technique is taylored for a particular truncated version of the 3/1 resonance and does not apply as such to the 2/1 resonance or to more precise models of the 3/1 resonance. Henrard and Lemaître (1987) first modified Wisdom's technique to apply it to the 2/1 resonance, then proposed a new semi-numerical approach (Henrard and Lemaître 1986) that did for the 2/1 resonance (see also Lemaître and Henrard 1989) what Wisdom's perturbative treatment did for the 3/1 resonance : explain in a theoretical frame the results of numerical integration by Giffen (1973), Froeschlé and Scholl (opus cited above) and Murray (1986).

The semi-numerical approach of Henrard and Lemaître is more general and can be applied to the 3/1 resonance as well. Even when applied to the 3/1 resonance truncated at the lowest order, it is not equivalent to Wisdom's perturbative treatment and a question immediately arises : how do they compare ?

This is the main question we would like to answer in this paper. The short answer will be : they compare well and both of them compare well with the "real world" (personified here by the numerical integration of the truncated differential equations). Both of them have their weaknesses (not always the same ones) and we do not find one of them to be much better than the other one.

Of course, the interest of the comparison is not only in the comparison itself. Beyond that, we would like to assess the effectiveness of the semi-numerical approach with the idea of applying it later to more refined models of the 3/1 resonance (to bring the "real world" closer to the real asteroids). We would like also to sharpen the analysis based upon a perturbative treatment by pointing out some aspects of it that were not emphasized in Wisdom's treatment. We think that the role of secondary resonances is the most important of these aspects.

The second section describes the Hamiltonian of the truncated (at degree two in eccentricities) averaged (over the orbital period) planar elliptic restricted three body problem at the internal resonance 3/1. This is the problem on which we can compare the two perturbation methods. We describe also briefly the way Wisdom transforms the Hamiltonian into a *Pendulum-like* Hamiltonian (see (9)). We contrast this with the way we propose to transform the Hamiltonian into a simpler *model Hamiltonian* (H_0 in (17)) plus a perturbation (H_1 in (17)). The model Hamiltonian we propose is the one of the circular restricted problem but its solution already contains part of the effect of Jupiter's eccentricity through a simple transformation (16), similar to the reducing transformation we have already used in the 2/1 resonance problem (Henrard *et al* 1986). A first comparison of the two methods with numerical results can already be performed at this stage and is summarized in Figure 2. It is based upon the identification (proposed by Wisdom) of the separatrices of the "fast-degree of freedom" (the pendulum or the model Hamiltonian) as the main generators of chaotic motion.

In Section 3, we perform the first step of our semi-numerical perturbation method by introducing the action-angle variables of the model problem and by computing the frequencies associated with the angular variables. The computation of the frequencies enables us to identify another possible generator of chaotic motion : the secondary resonances. They are the main generators of chaotic motion in the 2/1 resonance case and we shall see that they have also a role to play in the 3/1 resonance case.

The description of the semi-numerical perturbation method is continued in Section 4 with the description of the first order averaging. A short cut in the determination of the generating function enables us to compute very easily a "quasi-integral" of the motion at the cost of loosing the full potential accuracy of the method. Nevertheless a first comparison of the theoretical results with numerical integration is satisfactory.

In Section 5, we present the results of our perturbation method under the form of surfaces of section for five levels of energy. For three of them comparison can be made with similar surfaces of section obtained numerically by the mapping technique (Wisdom 1985). Unfortunately, Wisdom gives the theoretical surface of section obtained by his perturbative method for only one of them and even for this one leaves the central area blank (commenting in the text that the curves are distorted there). We find that the comparison is good in the resonance zone but that the level curves we obtain in the central area are badly distorted. Are they more distorted than Wisdom's ones ? We do not know but it is quite possible as Wisdom's neighbouring curves represent better the numerical results than ours. We attribute this defect of our technique to the approximation we made in the determination of the generating function. This approximation is indeed at its worst in this region of the phase space.

Wisdom's three surfaces of section are concentrated on the chaotic area at the edge of the resonance zone. We present another surface of section deeper in the resonance zone to show how the perturbation technique behaves in this regular region (Figure 11 and 12).

For the surfaces of section analysed in Section 5, the chaotic domains generated by the crossing of the separatrices and by the secondary resonance have merged together and it is difficult to assess their relative importance. We show and comment in Section 6 a case (obtained by decreasing the value of the eccentricity of Jupiter) where they are separated. As pointed out by Wisdom (1985), the separatrix crossing mechanism generates more chaos but nevertheless the secondary resonance chaotic layer is qualitatively important as it is responsible in this case for the random jumps between a high eccentricity mode and a low eccentricity mode.

2. The averaged planar elliptic problem for the 3/1 resonance

The Hamiltonian of the restricted three body problem can be written (see, for instance, Szebehely 1967) :

$$H = -\frac{1-\mu}{2a} - \mu \left\{ \frac{1}{|\vec{r}-\vec{r}'|} - \frac{\vec{r}\,|\,\vec{r}'}{r'^3} \right\} \tag{1}$$

where $(1-\mu)$ and μ are the reduced mass of the primary (the Sun) and secondary (Jupiter), a (resp. a'), $\vec{r}$ (resp. $\vec{r}'$) the semi-major axis and position vector (relative to the Sun) of the test particle (resp. of Jupiter). We are considering here that the Hamiltonian function (1) is expressed implicitely in the usual modified Delaunay's elements (λ, p, L, P) where the quantities L , P are the momenta respectively conjugated to the angular variables λ , p :

$$\begin{aligned} \lambda &= \text{mean longitude of the particle}, & L &= \sqrt{(1-\mu)a}\,, \\ p &= -(\text{longitude of its pericenter})\,, & P &= L(1-\sqrt{1-e^2})\,. \end{aligned} \tag{2}$$

The Hamiltonian is also a function of the time through its dependence upon

the mean longitude λ' of Jupiter. In case of a 3/1 resonance

$$3n' - n \simeq 0 \tag{3}$$

between the unperturbed mean motion of the test particle $n = [(1-\mu)/a^3]^{1/2}$ and the mean motion of Jupiter $n' = a'^{3/2}$ it is useful to introduce the Poincaré resonance variables

$$\begin{aligned} \sigma &= [3\lambda' - \lambda + 2p]/2\,, & S &= P\,, \\ \nu &= -[3\lambda' - \lambda + 2p']/2\,, & N &= 2L + P - 2\sqrt{(1-\mu)a^\star}\,, \end{aligned} \tag{4}$$

where $a^\star$ is the "exact resonance" value : $a^\star = [(1-\mu)/9]^{1/3}$, and to average the Hamiltonian (1) over the remaining fast variable which is essentially the time. This averaging is not just a rough approximation of the first order in μ but can be justified in terms of a transformation of coordinates from the osculating coordinates (4) to a set of "averaged" coordinates $(\bar\sigma, \bar\nu, \bar S, \bar N)$ (see, for instance Message 1966). In order to keep the notations as simple as possible, we shall drop the superscripts of the averaged variables and note them also (σ, ν, S, N) .

The averaging transforms the time dependent Hamiltonian (1) into a time-independent one. When expanded in powers of the eccentricities (e, e') and the difference $(a - a^\star)$ and written in terms of the canonical variables, this Hamiltonian reads

$$\begin{aligned} H \;= C(N-S)^2 + A'S \;& + 2D'S\cos 2\sigma + 2F'e'^2\cos 2\nu \\ & + e'\sqrt{2S}[E'\cos(\sigma-\nu) + G'\cos(\sigma+\nu)] \\ & + \cdots \end{aligned} \tag{5}$$

where the numerical coefficient C is of the order of unity and the other numerical coefficients (A', D', F', E', G') are of the order of the mass-ratio μ :

$$\begin{aligned} C &= -1.623564\,, & A' &= -0.410139\mu\,, \\ D' &= -0.863158\mu & F' &= -0.181477\mu\,, \\ E' &= \;\; 2.656407\mu & G' &= \;\; 0.198705\mu\,. \end{aligned} \tag{6}$$

The unperturbed (when $\mu = 0$) frequencies of the angular variables are

$$\dot\nu = -\dot\sigma = 2C(N-S) \tag{7}$$

from which it is obvious that the first three periodic terms in the perturbation (terms in 2σ , 2ν , $\sigma - \nu$) have the same unperturbed frequency while the last term (the secular term in $\sigma + \nu$) has a zero unperturbed frequency.

Of course, unperturbed frequencies are only first approximations but it is reasonable to assume, at least as a first guess to be confirmed a posteriori, that two natural time scales drive the motion : the time scale of σ (the resonant angle time scale) and the time scale of $\sigma + \nu = p - p'$ (the perihelion time scale). This is of course on top of the orbital time scale that we have averaged out.

To take advantage of this observation, Wisdom (1985) proposes to regroup the terms with the resonant angle time-scale into one cosine term modulated by the perihelion time-scale. Of course, this is possible because all these terms have the same unperturbed frequency. Introducing the canonical variables

$$\begin{aligned} \xi &= \sqrt{2S}\cos(\sigma+\nu)\,, & \eta &= \sqrt{2S}\sin(\sigma+\nu)\,, \\ \phi &= 2\nu\,, & \Lambda &= \tfrac{1}{2}(N-S)\,, \end{aligned} \tag{8}$$

brings the Hamiltonian (5) under the form

$$H = 4C\Lambda^2 + D'\mathcal{A}\cos(\phi - \mathcal{P}) + \frac{A'}{2}(\xi^2 + \eta^2) + G'e'\xi \tag{9}$$

with

$$\begin{aligned} D'\mathcal{A}\cos\mathcal{P} &= D'(\xi^2 - \eta^2) + e'E'\xi + 2F'e'^2 , \\ D'\mathcal{A}\sin\mathcal{P} &= 2D'\xi\eta + e'E'\eta . \end{aligned} \tag{10}$$

The restoring torque $\mathcal{A}$ can also be written under the more symmetric form (see Henrard 1988)

$$\mathcal{A}^2 = [(\xi - X_1)^2 + \eta^2][(\xi - X_2)^2 + \eta^2] \tag{11}$$

where X_1 and X_2 are the roots of the quadratic equation

$$D'X_i^2 + e'E'X_i + 2F'e'^2 = 0 . \tag{12}$$

The variable restoring torque $\mathcal{A}$ is the product of the distances in the plane (ξ, η) to two particular points on the ξ-axis :

$$\begin{aligned} X_1 &= 0.143e' &&= 0.007 , \\ X_2 &= 2.934e' &&= 0.141 . \end{aligned} \tag{13}$$

With respect to the (ϕ, Λ) degree of freedom (the degree of freedom corresponding to the resonant angle time-scale), the Hamiltonian (9) is the Hamiltonian of a pendulum. The frequency of its stable equilibrium

$$\omega_1 = [8CD'\mathcal{A}]^{1/2} = 3.348[\mu\mathcal{A}]^{1/2} \tag{14}$$

is representative of its time-scale.

The time scale of the (ξ, η) degree of freedom is more difficult to pinpoint but, looking at the differential equations governing it, we can estimate its basic frequency as :

$$\omega_2 = \mu \cdot \max[\xi, \eta, e'] . \tag{15}$$

The initial guess that the two time-scales are well-separated is thus confirmed (their ratio is approximatively $\mu^{1/2} \sim 0.03$) except of course in the vicinity of the peculiar points (13) and in the vicinity of the separatrix of the pendulum. Wisdom proposes then to consider the Hamiltonian (9) as a one-degree-of freedom Hamiltonian in (ϕ, Λ) , the coefficients of which vary slowly with time as (ξ, η) follow its orbit, and to use the adiabatic invariant theory together with the analytical formulae for the motion of the pendulum to further average the problem over the fast time scale (the time scale of the resonant angle).

The straightforward application of the adiabatic invariant principle (see Henrard 1989 for a review) to this case is not completely satisfactory. Indeed the small parameter which measures the first order invariance of the action should be estimated not only by the normalized time derivatives of the "parameters" $\mathcal{A}$ and $\mathcal{P}$ (here $\mu^{1/2} \sim 0.03$) but also by the square root of the normalized second time derivatives of these parameters (here $\mu^{1/4} \sim 0.18$ because the motion in ξ, η depends upon the resonant angle time scale).

An alternate, more rigorous, derivation of the technique has been proposed by Wisdom (1985) and later on formalized by Koiller *et al* (1987). It is based upon

the extension to two degrees of freedom of the one-degree-of freedom canonical transformation to the action-angle variables of the pendulum. As the "parameters" $\mathcal{A}$ and $\mathcal{P}$ of the pendulum depend in a rather involved way upon the (ξ, η) degree of freedom, this extension is not straightforward and only approximate formulae (of first order in $\mu^{1/2}/\mathcal{A}$) have been proposed.

The perturbation method that one of us has proposed for the 2/1 resonance problem (Henrard and Lemaître 1986) and that we wish to develop now in the context of the 3/1 resonance is actually very close to this last technique. It may be summarized by the aphorism : Let us not try to embrace the full problem at once. Let us define a model problem which would be of course as close as possible to the full problem but such that the interdependence of the two degrees of freedom is simple enough that action-angle variables can be defined easily for the two degrees of freedom.

In order to achieve this, we have to come back to the Hamiltonian (5) and propose instead of (8) the canonical transformation (where (x, M) are the momenta respectively conjugated to (y, ν))

$$\begin{aligned} x = \sqrt{2R}\cos r &= \sqrt{2S}\cos\sigma + \tfrac{E'}{2D'}e'\cos\nu\,, \\ y = \sqrt{2R}\sin r &= \sqrt{2S}\sin\sigma - \tfrac{E'}{2D'}e'\sin\nu\,, \\ \nu &= \nu\,, \\ M &= N - \tfrac{A'}{2C} + \tfrac{E'}{2D'}e'\sqrt{2S}\cos(\sigma+\nu) + \tfrac{1}{2}(\tfrac{E'e'}{2D'})^2\,. \end{aligned} \tag{16}$$

This transformation, which is related to the rotation in phase space introduced by Poincaré (1899) in the context of the secular perturbation of planets and by Sessin and Ferraz-Mello (1984) (see also Wisdom 1986, Henrard *et al* 1986) in the context of first order resonance is surprizingly useful. It introduces in a very simple way a kind of "free eccentricity" ($\sqrt{2R}$ instead of $\sqrt{2S} \sim e$) together with a kind of "forced eccentricity" ($\frac{E'}{2D'}e'$) . We shall call the angular variable $(r+\nu)$ the "recentered argument of the perihelion" because of its analogy with the angular variable $\sigma+\nu = p - p'$. By this, we can take into account at small cost a substantial part of the perturbation due to the eccentricity of Jupiter. Indeed the transformation (16) reduces the Hamiltonian function (5) to :

$$\begin{aligned} H &= H_0 + H_1 - 4.19153\,10^{-6}\,, \\ H_0 &= C(M-R)^2 + AM + 2DR\cos 2r\,, \\ H_1 &= Ge'\sqrt{2R}\cos(r+\nu) + 2Fe'^2\cos 2\nu \end{aligned} \tag{17}$$

with

$$\begin{aligned} C &= -1.6235638\,, & A &= -0.410139\mu\,, \\ D &= -0.863158\mu & F &= +0.840424\mu\,, \\ G &= -0.432405\mu\,. \end{aligned} \tag{18}$$

If we compare (17) with the original Hamiltonian (5) , we see that we have eliminated the large term in $E'\cos(\sigma-\nu)$. In order to compare the "model" H_0 in (17) with the Hamiltonian (9) , we compute in the new variables (16) the periodic term of the pendulum

$$D'\mathcal{A}\cos(\phi - \mathcal{P}) = 2DR\cos 2r + 2Fe'^2\cos 2\nu\,. \tag{19}$$

It appears that we have included in H_0 a much simplified version of this term ($2DR\cos 2r$ is actually independent of the other degree of freedom) at the cost of

rejecting part of it (the $2Fe'^2 \cos 2\nu$ term) in a "perturbation" function H_1 . This cost is almost negligible. Indeed, the other perturbative term, $Ge'\sqrt{2R}\cos(r+\nu)$, although it is long periodic, contains also small short periodic variations (as we have pointed out earlier while discussing the application of the adiabatic invariant) and these variations are usually larger than the term $2Fe'^2 \cos 2\nu$.

The model problem H_0 is now very simple. It is a one-degree-of-freedom model depending upon a parameter M (the perturbation will of course make M vary with time). It is actually the Hamiltonian corresponding to the circular restricted problem although by the reducing transformation (16) it takes into account part of the perturbation due to the eccentricity of Jupiter. It has been analysed in detail by Borderies and Goldreich (1986) and by Lemaître (1986) in the context of the adiabatic invariant theory. Trajectories of this problem for typical values of the parameter M are given in Figure 1 in the phase space plane $x = \sqrt{2R}\cos r$, $y = \sqrt{2R}\sin r$.

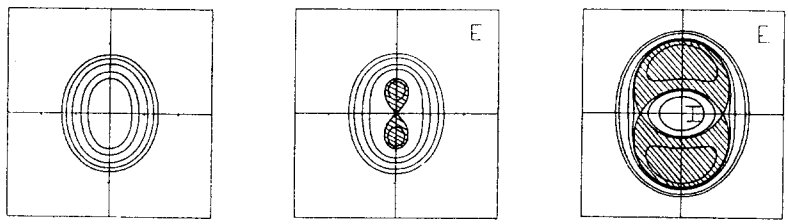

Fig. 1. Typical phase portrait of the Hamiltonian H_0 in the plane $\sqrt{2R}\cos r$, $\sqrt{2R}\sin r$. The first figure is for $M<-D/C$, the second one for $-D/C<M<D/C$ and the third one for $D/C<M$. The resonance zone is shaded.

Let us point out the existence of separatrix orbits, doubly asymptotic to unstable equilibria. These separatrices divide the three dimensional space (x, y, M) into three zones. An *internal zone* inside the smallest separatrix for $M > D/C$ (marked I in Figure 1). An *external zone* outside the largest separatrix for $M > -D/C$ (marked E in Figure 1) to which we add the full (x, y) space for $M < -D/C$ and a *resonance zone* in between the separatrices (shaded in Figure 1).

These separatrices play the same prominent role in our analysis as the separatrices of the pendulum in Wisdom's analysis. They will act as generators of chaotic motion.

Before going further, it may then be worthwile to check whether the separatrices fall in the right place : i.e. in the chaotic region as determined numerically by Wisdom. Figure 2a (resp. Figure 2b) shows the intercepts of the separatrices (see the second and third frames of Figure 1) of our model Hamiltonian H_0 (resp. of Wisdom's pendulum) with the "representative plane" $(a, e\sin\sigma)$ which is the junction of the two "representative half planes" used by Wisdom (1983-1985) and Murray and Fox (1984).

This plane is defined as the intersection of the phase space (y, x, ν, M) with the hyperplane $\nu = \pi/2$ and the hyperplane $x = 0$. This plane is mapped on the plane $(a, e\sin\sigma)$ through the inverses of the transformations (16), (4) and (2). Notice that, for $x = 0$, the $\sin\sigma$ may take only the values $+1$ or -1 . Hence the value of e may be read directly from the diagram as the absolute value of the ordinate $e\sin\sigma$.

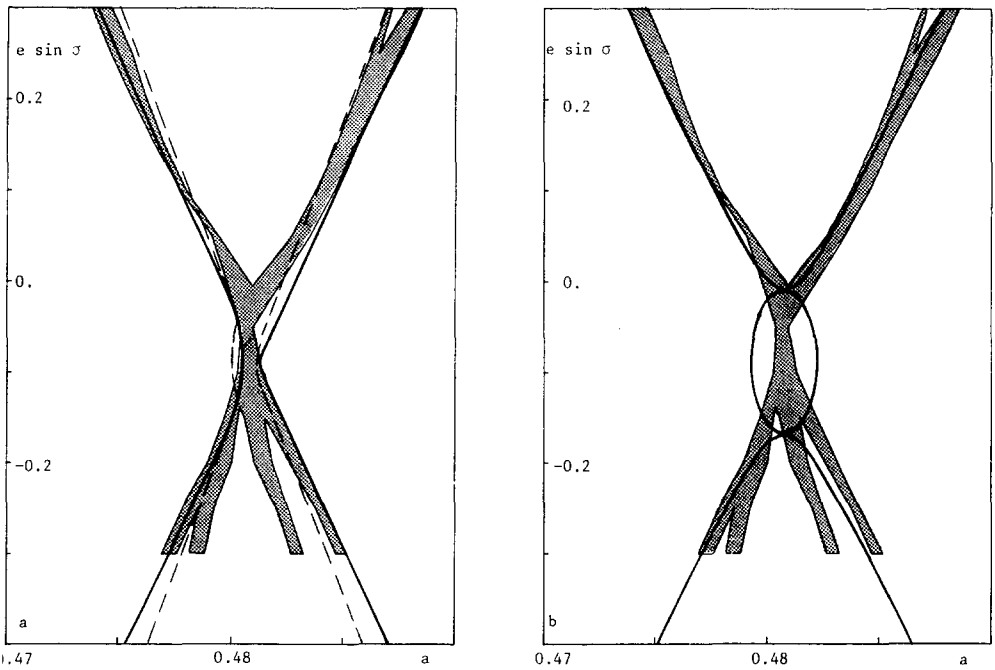

Fig. 2. The traces of the separatrices in the representative plane $(a, e\sin\sigma)$. Figure a is for the separatrices of the model problem H_0 and Figure b for the separatrices of the pendulum (equation (9)). The initial conditions of chaotic trajectories (as determined numerically by Wisdom 1983) are shown shaded. Also shown in Figure 2a as dashed curves are the locations where the main secondary resonances are expected (see Section 3). Note that the internal zone is to the right of Figure 2a, the external zone to the left and the resonance zone in the middle.

The agreement is good although not perfect. Quite surprizingly the separatrices of H_0 (Figure 2a) may look as a better "backbone" to the chaotic region than the separatrices of the pendulum (Figure 2b).

Also shown in Figure 2a (as dashed curves) are the main secondary resonances as computed in Section 3. We shall see later on that they are at the same time the center of islands of regular motion (at the bottom of Figure 2a) and the generator of chaotic motion (at the top of Figure 2a). Here also the agreement is good. The secondary resonances as predicted by our perturbative method fall nicely in the two prongs of regular motion at the bottom of Figure 2a and help to explain the existence of these two prongs. At the top of Figure 2a, the secondary resonances mark the boundary of the chaotic region.

3. A semi-numerical perturbation method : The frequencies

Let us introduce action-angle variables for the one-degree-of-freedom Hamiltonian H_0 (see (17)). Action-angle variables are usually introduced by means of a generating function, but, except in very simple cases, this leads to implicit expressions and complex integrals which cannot be solved analytically. We prefer to introduce

them in the following way which leads directly to a semi-numerical implementation (see Henrard and Lemaître 1986). Let

$$\begin{aligned} y &= Y'(y_0, t, M) , \\ x &= X'(y_0, t, M) \end{aligned} \tag{20}$$

be the solution of the differential equations associated with the Hamiltonian H_0 in the phase space $y = \sqrt{2R}\sin r$, $x = \sqrt{2R}\cos r$. The solution is a periodic function of the time t of period $T(y_0, M)$ and depends also upon the initial conditions $(x = 0, y = y_0)$ and the parameter M . In general we should allow for both initial conditions (x_0, y_0) to be considered but in the context of the 3/1 resonance we can and we will always choose $x_0 = 0$.

The action-angle variables can then be defined and numerically estimated by

$$\psi = \frac{2\pi}{T} t , \quad J = \frac{1}{4\pi} \int_0^T (X' \frac{\partial Y'}{\partial t} - Y' \frac{\partial X'}{\partial t}) \, dt . \tag{21}$$

The action J is computed as a function of y_0 and M in (21). This function can be numerically inverted to write, by substitution, the solution (20) under the form :

$$\begin{aligned} y &= Y(\psi, J, M) , \\ x &= X(\psi, J, M) . \end{aligned} \tag{22}$$

This is a one-degree-of-freedom canonical transformation depending upon a parameter M . But we wish to consider M as the momentum of a second degree of freedom. The extension of (22) to a two degree of freedom canonical transformation leads to

$$\begin{aligned} y &= Y(\psi, J, M) , \\ x &= X(\psi, J, M) , \\ \nu &= m + \rho(\psi, J, M) , \\ M &= M \end{aligned} \tag{23}$$

with

$$\rho = \int_0^{\psi} (\frac{\partial X}{\partial \psi'} \frac{\partial Y}{\partial M} - \frac{\partial X}{\partial M} \frac{\partial Y}{\partial \psi'}) \, d\psi' . \tag{24}$$

Details about the properties of the function ρ are given in Henrard and Lemaître (1986). In general a function of (J, M) should be added to the expression (24) but this function vanishes here (as it vanished in the problem investigated in Henrard-Lemaître 1986) because of symmetries of the problem. It is enough to recall here that the function ρ can be evaluated numerically at the same time that the solution (20) is computed by integrating simultaneously the variational equations, and that a proper choice of the initial conditions for the variational equations makes the function ρ a 2π-periodic function of ψ .

We have insisted on the fact that the transformation (23) can be computed numerically at any point. The same is true for its derivatives (see Henrard and Lemaître 1986). This is because we want to stress the point that is it as useful from a practical point of view as an analytical expression (except that it may take more computer time depending on the complexity of the analytical expression to which it is compared).

But we shall see that actually the perturbation scheme can be arranged in such a way that we shall never need to evaluate the transformation.

Substituting (23) into the Hamiltonian (17) we find :

$$\begin{aligned} &K = K_0 + K_1 \ , \\ &K_0(J, M) = H_0(Y(\psi, J, M), X(\psi, J, M), M) \ , \\ &K_1(J, M, \psi, m) = H_1(Y(\psi, J, M), X(\psi, J, M), m + \rho, M) \ . \end{aligned} \tag{25}$$

This Hamiltonian is now almost ready for the application of a classical perturbation theory, having a main part K_0 which depends only upon the momenta, and a periodic perturbation part K_1 .

We say "almost ready" because we have still to check whether the two "unperturbed" frequencies

$$\omega_1 = \frac{\partial K_0}{\partial J} \qquad , \qquad \omega_2 = \frac{\partial K_0}{\partial M} \tag{26}$$

are in resonance or not.

These frequencies are easy to compute along any trajectory of the model problem H_0 . We have

$$\omega_1(J, M) = \frac{2\pi}{T} \ , \quad \omega_2(J, M) = \frac{1}{T} \int_0^T \frac{\partial H_0}{\partial M} \, dt \tag{27}$$

where T is the period of the trajectory labelled by the value of J and M .

We show in Figure 3 the curves $\omega_2/\omega_1 =$ constant, not in the plane (J, M) which is not very suggestive but in the "representative plane" $(a, e \sin \sigma)$.

Figure 3 is obtained by parametrizing by their semi-major axis and eccentricity the points on the axis $x = 0$ (for different values of M). Then these points are taken as initial conditions of orbits of the model Hamiltonian H_0 (see Figure 1) along which the expressions (27) are evaluated. Notice that we do not have to evaluate explicitely the action-angle transformation (23). We just have to integrate numerically the periodic orbits, find their period, and evaluate an integral along them. This integral can be evaluated by appending to the differential equations in x and y a third equation :

$$\dot{z} = \frac{\partial H_0}{\partial M} \, (y, x, M) = A + 2CM - C(x^2 + y^2) \ . \tag{28}$$

The value of ω_2 is then the end-value of z divided by the period T .

The first thing we notice in Figure 3 is the discontinuity between the three zones (internal, resonance and external). Indeed the transformation (23) to action-angle variables is singular along the separatrices. The singularity is a logarithmic one (see Henrard 1989 for an analysis) so that we have to come very close to the separatrices for things to go really bad, but the singularity exists and is such that the transformation (23) looks more like three separate transformations each one acting in a separate region of the phase space.

The frequency ω_2 , which is the mean motion of the angular variable ν is small in the resonance zone. Indeed, as r librates in this zone, the mean motion of ν is the mean motion of the recentered perihelion (as in Section 2, we call recentered perihelion the angular variable $r+\nu$; the true perihelion is given by $p-p' = \sigma+\nu$). On the other hand, in the internal and external zones, the angular variable r circulates and the mean motion of ν is equal to the mean motion of r plus the mean motion of the recentered perihelion. Hence ω_2 is close to the absolute value

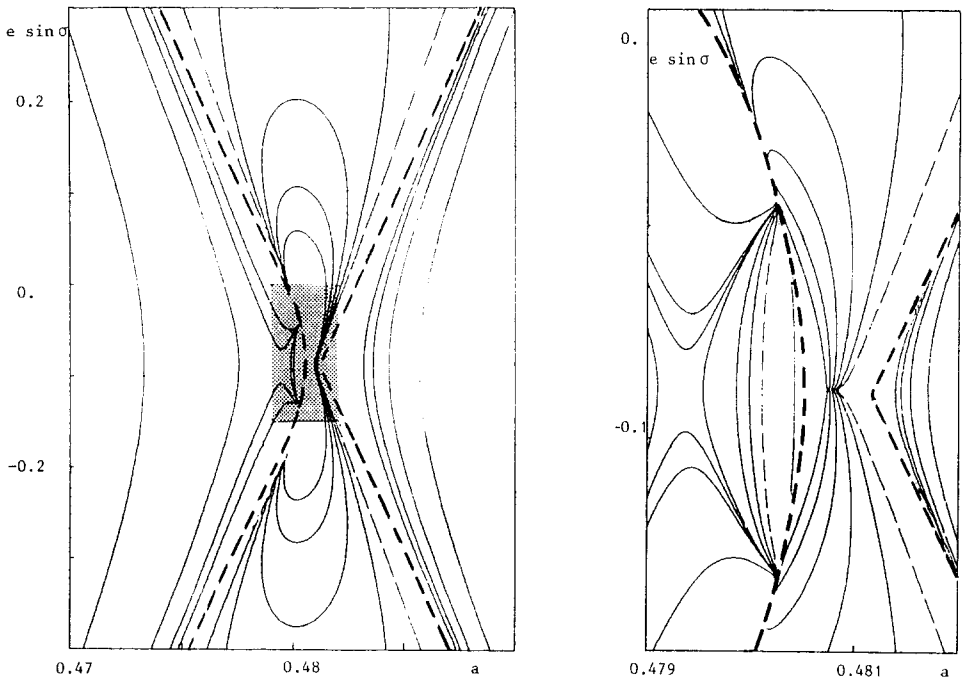

Fig. 3. The ratio of frequencies in the representative plane $(a, e\sin\sigma)$. The plane is divided into three zones by the trace of the separatrices (heavy dashed curves) of the model problem H_0 . The level curves are from the left to the right ω_2/ω_1 =0.99, 0.98, 0.97, 0.96 (in the external zone), ω_2/ω_1 =0, 0.025, 0.05, 0.075, 0.1 (in the resonance zone) and ω_2/ω_1 =−1.05, −1.04, −1.03, −1.02 (in the internal zone). Figure 3b is a close-up of the shaded region of Figure 3a and shows for the external zone the level curves : ω_2/ω_1 =1.1, 1., 0.99, 0.98, 0.972, 0.971, 0.97, 0.96 (from the right to the left and then up and down beyond the saddle point). For the resonance zone, the level curves ω_2/ω_1 =0.5, 0.4, 0.3, 0.2, 0.1, 0 (from the left to the right) and for the internal zone, the level curves ω_2/ω_1 =−1.5, −1.4, −1.3, −1.2 (from the left to the right). The curves for which $\omega_2/\omega_1 = 0$ (in the resonance zone) or $\omega_2/\omega_1 = 1$ (in the external zone) correspond to zero mean motion of the recentered perihelion and are shown dashed.

of ω_1 , the mean motion of r (which is the same as the mean motion of ψ). The change in sign between the internal and external zones reflects the change of sign of the mean motion of r .

The mean motion of the recentered perihelion can then be recoved by the formula

$$\omega_p = \omega_2 + i_z\omega_1 \tag{29}$$

where i_z, the *index of the zone* is set at

$$\begin{aligned} i_z &= 0 && \text{in the resonance zone ,} \\ i_z &= 1 && \text{in the internal zone ,} \\ i_z &= -1 && \text{in the external zone .} \end{aligned} \tag{30}$$

From Figure 3, it appears that the mean motion of the recentered perihelion vanishes along two curves, one completely in the resonance zone and the other one partly in the resonance zone and partly in the external zone. These curves are shown as dashed curves in Figure 3 and are reproduced in Figure 2a. Along these curves we expect a resonance phenomenon as we have indicated at the end of the preceeding section. The structure of this resonance phenemenon will be revealed in the surfaces of section computed in the next section.

As ω_1 becomes smaller close to the separatrices (the period of the orbits becomes larger), the ratio ω_p/ω_1 becomes larger and we may expect other secondary resonances between these two frequencies. As a matter of fact the innermost level curve in the resonance zone of Figure 3a corresponds to a commensurability $\omega_p/\omega_1 = 1/2$. But as these secondary resonances are squeezed along the separatrices, they certainly overlap and they do not reveal themselves as separate resonances but as a layer of chaotic motion. This is one way of explaining in this context that the separatrices act as generators of chaotic motion. Another way, which leads naturally to estimates of the size of the layer and of the diffusion coefficient inside the layer, rely on estimates of the change in the adiabatic invariant due to the crossing of the separatrix. We shall come back on this later on.

We are now in a position to compare qualitatively the behavior of the 3/1 resonance with the behavior of the 2/1 resonance as it has been analysed by Henrard-Lemaître (1986) and Lemaître-Henrard (1989).

In the 2/1 resonance, the separatrices of the model problem (a modification of the circular restricted problem as it is here) were found also to match closely one of the layer of chaotic motion discovered numerically by Murray (1986) and confirmed by Wisdom (1987). Similarly a curve along which ω_p vanishes was found in the representative plane and this curve runs also along and close to the separatrix curve. This curve was identified with another layer of chaotic motion in Murray's diagram.

But the cause of the largest layer of chaotic motion in the 2/1 resonance was found to be secondary resonances between the two main frequencies. These secondary resonances are standing alone far away from the separatrix curve while we have just seen that in the 3/1 resonance they follow closely the separatrix curve.

In retrospect, this could have been expected. The point is that in a first order resonance, like the 2/1 resonance, the separatrix curve is *discontinuous*. If secondary resonances follow it (as they do), they have to "bridge the gap" between the two pieces of the separatrix curve and thus stand alone to form a rather large layer of chaotic motion. In a paradoxal way, it is the *absence of separatrix* which is responsible for the largest area of chaotic motion in the 2/1 resonance while in the 3/1 resonance, the secondary resonances are always kept in line by the separatrices.

4. A semi-numerical perturbation method : The averaging

As we have recognized that the combination of frequencies $\omega_p = \omega_2 + i_z\omega_1$ vanishes on some curves (see previous section) and furthermore is rather small in most of the domain of interest, we shall again change variables to introduce the corresponding

angular variable. Let us consider the canonical transformation :

$$\begin{aligned} \psi &= \psi \,, & \Psi &= J - i_z M \,, \\ q &= m + i_z \psi \,, & Q &= M \,, \end{aligned} \tag{31}$$

where, by (30), the quantity i_z is equal to zero in the resonance zone, to one in the internal zone and to minus one in the external zone. We could call the variable q , the "pseudo-perihelion". It differs from the recentered perihelion by short periodic terms only.

By the Lie transform method, a first order perturbation theory of the Hamiltonian (25) consists in defining a canonical transformation from the phase space (ψ, q, Ψ, Q) to the averaged phase space $(\bar{\psi}, \bar{q}, \bar{\Psi}, \bar{Q})$, the first order expression of which is

$$\begin{aligned} \bar{\psi} &= \psi - \frac{\partial W}{\partial \Psi} \,, & \bar{q} &= q - \frac{\partial W}{\partial Q} \,, \\ \bar{\Psi} &= \Psi + \frac{\partial W}{\partial \psi} \,, & \bar{Q} &= Q + \frac{\partial W}{\partial q} \,. \end{aligned} \tag{32}$$

The generating function W is considered as a small quantity (together with its partial derivatives) and is defined by the partial differential equation

$$\left(\frac{\partial K_0}{\partial \Psi}\right) \frac{\partial W}{\partial \psi} + \left(\frac{\partial K_0}{\partial Q}\right) \frac{\partial W}{\partial q} = K_1(J, M, \psi, q - i_z \psi) - \bar{K}_1(J, M, q) \,. \tag{33}$$

The function $\bar{K}_1$ is the new Hamiltonian in the "averaged" variables $(\bar{\psi}, \bar{q}, \bar{\Psi}, \bar{Q})$ and is itself defined as the average of K_1 over the "fast" angular variable ψ :

$$\bar{K}_1 = \frac{1}{2\pi} \int_0^{2\pi} K_1(J, M, \psi, q - i_z \psi) \, d\psi \,. \tag{34}$$

We cannot, in general, average over the pseudo-perihelion because its unperturbed frequency,

$$\frac{\partial K_0}{\partial Q} = \frac{\partial K_0}{\partial M} + i_z \frac{\partial K_0}{\partial J} \tag{35}$$

is close to zero.

An approximate solution W' of (33) can easily be found by ignoring the small term in $(\partial K_0 / \partial Q)$

$$W' = \left(\frac{\partial K_0}{\partial J}\right)^{-1} \int_0^{\psi} [K_1 - \bar{K}_1] \, d\psi \,. \tag{36}$$

The exact solution W of (33) differs from this approximation W' by terms of the order of $[K_1 - \bar{K}_1](\frac{\partial K_0}{\partial Q})(\frac{\partial K_0}{\partial J})^{-2}$. This is actually the principal source of error in our perturbation scheme. It could be avoided by Fourier-analyzing the function K_1 , but it simplifies so much the computations (see (37) below) that we felt it is worth it.

Indeed, if we now evaluate the transformation (32) at $\psi = 0$, we find that all derivatives of W vanish except the derivative with respect to ψ which takes a very simple form. The function $\bar{\Psi}(\psi, q, \Psi, Q)$ which is an (approximate) integral of the problem because the new Hamiltonian $\bar{K}_1$ does not depend upon its conjugate

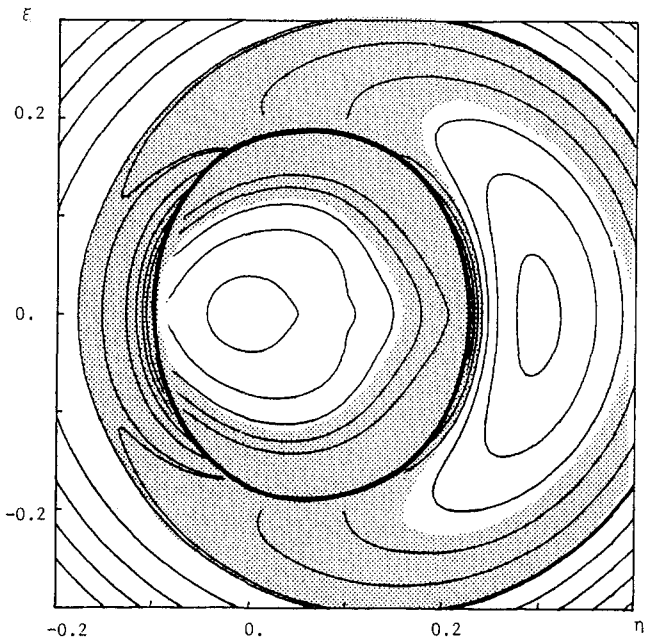

Fig. 4. Level curve of the quasi-integral $\bar{\Psi}$ on one sheet on the surface of section $\psi=0$, $H=-2.10^{-5}$ projected on the plane (ξ, η) . The thick curve is the trace of the separatrix surface.

variable $\bar{\psi}$ (at least to the first order), takes when evaluated at $\psi = 0$, the simple form

$$\bar{\Psi}(0, q, \Psi, Q) = J - i_z M + (\frac{\partial K_0}{\partial J})^{-1}[K_1(J, M, 0, q) - \bar{K}_1(J, M, q)] . \qquad (37)$$

In order to draw Poincaré's diagram on the surface of section $(H = h_0, \psi = 0)$, all we need is to be able to evaluate the function (37) at any point of the surface of section.

Pick a point on the surface of section, which we shall parametrize by the values of ξ and η (see (8)). The definition of the surface of section $(\psi = 0)$ makes $x = 0$ (see (16)) and we can deduce the corresponding values of y and ν . The value of M is then extracted from the equation $H = h_0$.

For the initial conditions $(x = 0, y)$, we compute the periodic orbit of the model problem H_0 , together with the integral J (see (21)). The period of the orbit is equal to $2\pi(\partial K_0/\partial J)^{-1}$. The value of K_1 is just the value of H_1 (see (17)) at the initial point. It remains to evaluate $\bar{K}_1$ from (34).

Taking into account that

$$\begin{aligned} K_1 &= e'G(x\cos\nu - y\sin\nu) + 2Fe'^2\cos 2\nu \qquad (38) \\ &= e'G[x\cos(q+\tilde{\rho}) - y\sin(q+\tilde{\rho})] + 2Fe'^2\cos 2(q+\tilde{\rho}) \end{aligned}$$

with

$$\tilde{\rho} = \rho(\psi, J, M) - i_z\psi \qquad (39)$$

where ρ has been defined in (24), we find easily that

$$\overline{K_1} = \overline{S_1} \sin q + \overline{C_2} \cos 2q \ . \tag{40}$$

The terms in $\cos q$ and $\sin 2q$ have disappeared from $\overline{K_1}$ because of the symmetries of the periodic orbits of the model problem H_0 (which are such that $x(\psi) = -x(-\psi)$, $y(\psi) = y(-\psi)$ and $\tilde{\rho}(\psi) = -\tilde{\rho}(-\psi)$) and the coefficients of the remaining terms are :

$$\begin{aligned} \overline{S_1} &= -\tfrac{e'G}{T} \int_0^T (x \sin \tilde{\rho} + y \cos \tilde{\rho})\, dt \ , \\ \overline{C_2} &= \tfrac{2Fe'^2}{T} \int_0^T (\cos 2\tilde{\rho})\, dt \ . \end{aligned} \tag{41}$$

Indeed ψ is just a scaled avatar of the time. We have now all the pieces to compute the integral (37) if we take into account that, when $\psi = 0$, $q = m = \nu$.

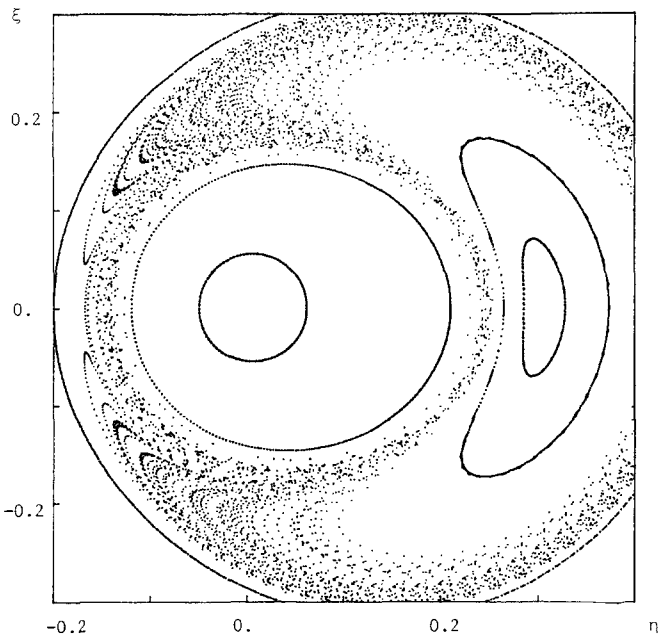

Fig. 5. Same surface of section as in Figure 4 but obtained by numerical integration. The chaotic trajectory was computed for 4.10^6 years, the regular trajectories for 1.10^6 years.

We show in Figure 4, the level curves of the function $\bar{\Psi}$ (see (37)) on the surface of section ($\psi = 0$, $H = -2.10^{-5}$).

The first thing we notice is the discontinuity accross the thick curve. This last one is not a level curve of the integral but the trace on the surface of section of the separatrix surface we discussed in Section 3. Indeed, as we have seen, the angle-action transformation (23) is singular along this separatrix surface and so is $\bar{\Psi}$. The adiabatic invariant theory (the application of which is not straightforward in this context as we have mentioned but which can still be used as a guide-line) tells us that when an orbit approaches the separatrix along a given level curve, the action $\bar{\Psi}$ experiences a (small ?) random jump. The succession of jumps at each

crossing of the separatrix does eventually dissolve all the level curves crossing the separatrix into one large chaotic domain. We have shaded in Figure 4 the area containing the level curves which cross in this way the separatrix. This is done by simple inspection of the figure.

We notice also in the resonance zone (outside the separatrix curve in Figure 4), that the level curves take on the characteristic shape of a first order resonance, with a maximum of $\bar{\Psi}$ at around $(\xi = 0.3, \eta = 0)$ and a saddle point at around $(\xi = -0.15, \eta = 0)$. This is the secondary resonance $\omega_p = 0$ (see (29)) and, as we have mentioned at the end of Section 2, it is the cause of an island of regular motion (around the maximum of $\bar{\Psi}$) and the generator of chaotic motion surrounding it (in the vicinity of the saddle point).

Figure 5 shows the same surface of section but this time obtained by numerical integration of the equations of motion corresponding to the original Hamiltonian (17).

The agreement is excellent. The regular trajectories are well represented by the perturbative analysis. The chaotic domain is well predicted by the rules of thumb we have just mentioned (crossing of the sepatrix and vicinity of the saddle point). Compare the shaded area of Figure 4 and the chaotic orbit of Figure 5.

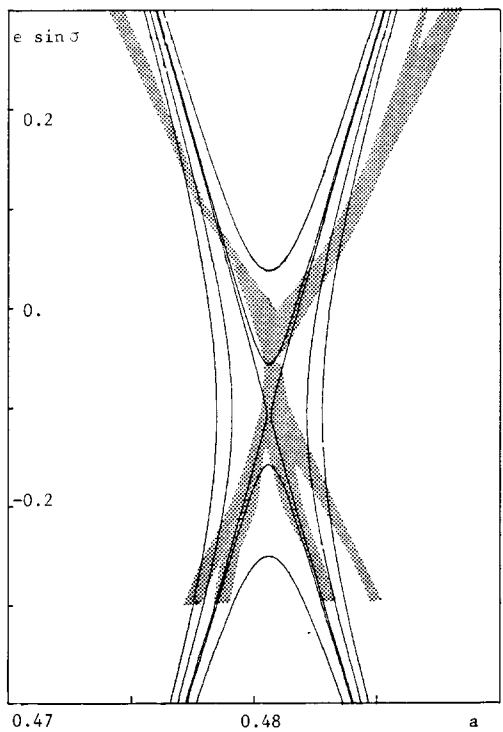

Fig. 6. Level curves $\Delta H = -2.10^{-5}$, $-1.21\ 10^{-5}$, $-4.22\ 10^{-6}$, $-3.04\ 10^{-6}$, 5.10^{-6} on the representative plane $(a, e \sin \sigma)$. Notice how these level curves look like hyperbolae. The highest level shown (5.10^{-6}) is at the top and bottom and the lowest one (-2.10^{-5}) on the left and right. Also shown as a shaded domain are the initial conditions of chaotic orbits as determined numerically by Wisdom (1983).

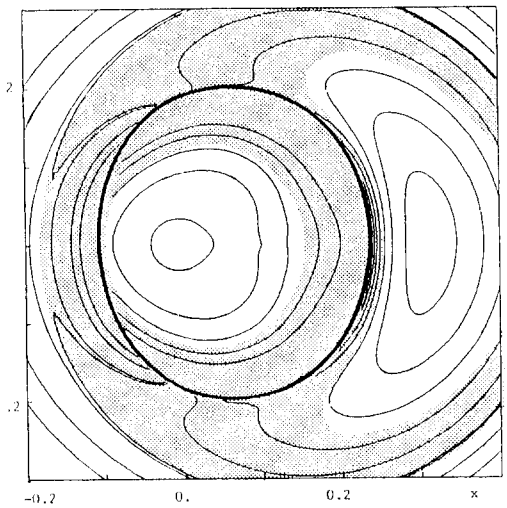

Fig. 7. Level curves $\bar{\Psi}=$ constant on the surface of section $\phi-\mathcal{P}=\pi$ and $\Delta H=-2.10^{-5}$. The thick curve is the trace of the separatrix surface.

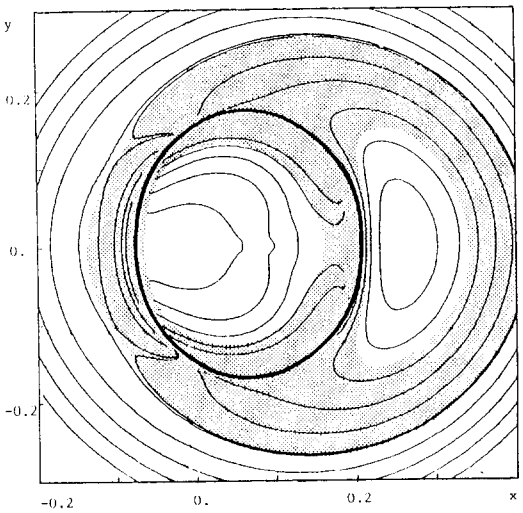

Fig. 8. Same as Figure 7 for $\Delta H=-1.21\ 10^{-5}$.

5. Surface of section : Comparison with Wisdom's results

In order to illustrate his perturbative technique, Wisdom (1985) chooses a surface of section slightly different from the one we have defined in Section 4.

First, in the definition of the surface of section, he chooses a different expression of the Hamiltonian than the expression H (see (5)) to which his perturbation method applies. This expression ΔH of the Hamiltonian differs from H in that the two body term (the first term in (1)) is not truncated as in (5). This is slightly inconsistent but does not make much difference. Secondly, the surface of section is not defined by $\psi = 0$ (or $2r = \pi$) but by $\phi - \mathcal{P} = \pi$ (see (9)). Again this does not make much difference except when R is small (see (19)).

In order to compare our results with Wisdom's results, we have modified the scheme described in the preceeding section. The initial conditions (ξ, η, M, ν) of points on Wisdom's surface of section are computed by using ΔH instead of H and are then mapped by numerical integration onto our surface of section ($\psi = 0$) where we can evaluate the quasi-integral $\bar{\Psi}$.

Before going further, it may be useful to describe the topology of these two dimensional surfaces of section, embedded in a four dimensional phase space. We present in Figure 6 the trace of the surfaces $\Delta H =$ constant onto the representative plane $(a, e\sin\sigma)$. Notice that the representative plane corresponds to the ξ-axis ($\eta = 0$) of the surface of section in Figures 4 and 5.

Let us consider that the condition $\psi = 0$ defines a three dimensional space parametrized by (ξ, η, a) . The representative plane is then a section $\eta = 0$ of this space and the surfaces of section $\Delta H =$ constant are approximately the hyperboloids obtained by rotating Figure 6 around an axis parallel to the "a"-axis and

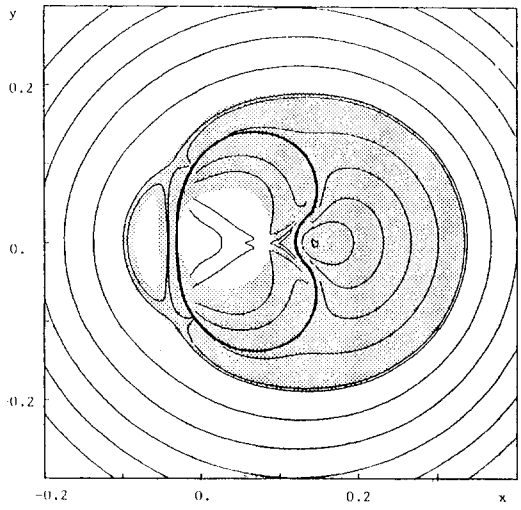

Fig. 9. Same as Figure 7 for $\Delta H = -4.22\ 10^{-6}$.

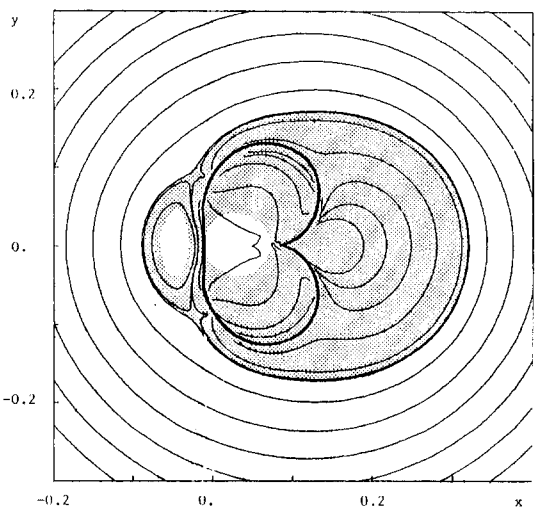

Fig. 10. Same as Figure 7 for $\Delta H = -3.04\ 10^{-6}$.

passing through the center of symmetry of Figure 6.

When ΔH is smaller than about $-4.2\ 10^{-6}$, the hyperboloid is a two-sheeted hyperboloid. Each sheet is disconnected from the other one and possesses a one-to-one projection on the (ξ, η) coordinate plane. Following Wisdom, we have chosen in Figures 4 and 5 to map only the left sheet, the one on the side of the external orbits. We are then missing all the internal orbits which remain for all time on the right sheet but we do encounter the resonance and chaotic orbits which cross alternatively the two sheets. In any case, the orbit which crosses one sheet draws on it a pattern disconnected from the pattern it may draw on the other sheet and the topology of this pattern is preserved by projection on the (ξ, η) coordinate plane.

But the situation is different when ΔH is larger than $-4.2\ 10^{-6}$. The hyperboloid is then a one-sheeted hyperboloid and the two patterns are no longer disconnected.

At the same time, the projection of the surface of section on the (ξ, η) plane shows a forbidden region (the hole in the hyperboloid).

If we cut the hyperboloid along the boundary of the forbidden region and project only the left-side of it on the (ξ, η) plane, the invariant curves may not close (part of them may be traced on the right side of the hyperboloid). If we choose to project both sides of the hyperboloid, curves may cross each other although they do not cross on the hyperboloid itself. It is the *projection* of a curve on the left side which crosses the *projection* of a curve on the right side.

Such surfaces of section are perfectly valid and have been used by many authors but of course their interpretation may be more difficult and sometimes confusing. We always have to remember that what we see on a diagram is only a projection of a surface which may not be topologically equivalent to a plane.

Wisdom criticizes the use of such surfaces of section by Giffen (1973), Scholl and

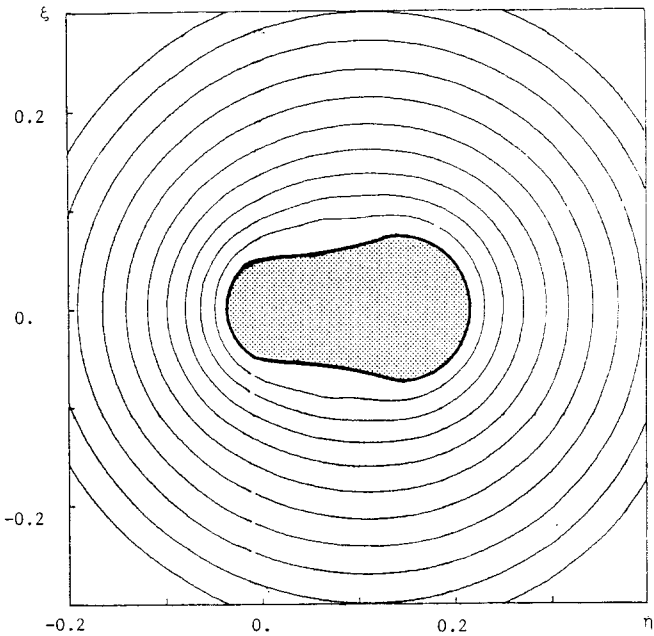

Fig. 11. Same as Figure 7 for $\Delta H = 5.10\ 10^{-6}$. The thick curve is no longer the trace of the separatrix surface but the boundary of the forbidden zone.

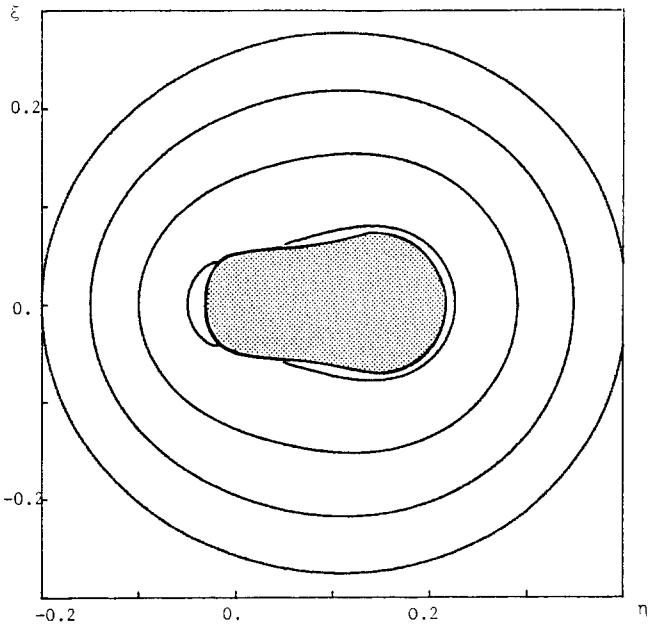

Fig. 12. Same surface of section as Figure 11 but obtained by numerical integration.

Froeschlé (1974, 1975) and Froeschlé and Scholl (1976, 1977, 1981). He motivates his use of a different surface ($\phi - \mathcal{P} = \pi$) by the fact that it projects better on the (ξ, η) plane. Indeed it does for the particular values of ΔH he investigates but,

for ΔH larger than $-2.72\ 10^{-6}$, the same phenomenon occurs and the projection of the surfaces of section $\phi - \mathcal{P} = \pi$ on the (ξ, η) plane presents also a forbidden zone (see Figure 11).

We show in Figures 7 to 11, the level curves $\bar{\Psi}$ = constant on the surface of section $\phi - \mathcal{P} = \pi$ for the values of ΔH shown in Figure 6.

The first value is the one used in Figure 4. Comparison of Figure 4 with Figure 7 shows that the two surfaces of section are very similar.

The next three values are the same as the one used by Wisdom (1985) and Figures 8, 9 and 10 should be compared with the numerically integrated surfaces of section (Figure 9, 10 and 11 of Wisdom 1985). Figure 9 can also be compared with Wisdom's theoretical surface of section (Figure 12 of Wisdom 1985).

The comparison is rather good in the resonance zone (outside the thick curves which represent the separatrix surface) but our level curves in the external zone (inside the thick curves), especially in Figure 9 and 10, are badly distorted and do not approximate the curves obtained by numerical integration. We attribute this to the fact that for these values of the energy and in this region of the phase space the errors due to the approximate character of the generating function (36) are overwelming. Indeed we are there well inside the shaded region of Figure 3 where the approximation $\omega_p \sim 0$ is very bad and where the values of $(\partial K_0/\partial J)$ is small (of the order of 0.005 and smaller).

Wisdom's perturbative method suffers also in this region from the smallness of $\mathcal{A}$ and he states that the curves "becomes distorted". As he does not represent them in his Figure 12 (the corresponding area is left blank), we cannot decide whether his perturbative method represents better this region than ours. This is not unlikely as the shape of the small island (just outside the thick curve on the left) is better represented in his Figure 12 than in our Figure 9.

We show also in Figure 11 a surface of section which lies deeper in the resonance zone ($\Delta H = 5.10^{-6}$). The separatrix surface does not cross this surface of section. The secondary resonance $\omega_p = 0$ is also absent. The causes of chaotic behavior have disappeared and all the trajectories are regular. This is confirmed by the results of the numerical integration shown in Figure 12. Notice in Figure 12 how the innermost invariant curve stops on the boundary of the forbidden zone to reappear further away. We are missing there a piece of the invariant curve which is on the other side of the hyperboloid.

6. The two generators of chaotic behaviour

We have explained in Section 5 why we believe that the chaotic behaviour found in this problem comes from two distinct sources : the slow crossing of the separatrices of the model problem H_0 (called slow Hamiltonian chaos by Escande (1985) or zone of uncertainty by Wisdom (1985)) and the separatrices of the secondary resonance $\omega_p = 0$ (Chirikov's separatrix layer). For the surfaces of section we have analysed, the two chaotic domains have merged together so it is difficult to determine which is the more important. From a surface of section corresponding to a problem with $A' = G' = 0$ (see (5)), Wisdom (1985) concludes that the Chirikov separatrix layer of the secondary resonance is not important.

The question may also be addressed, in a more natural way, by decreasing the value of the eccentricity of Jupiter. If we take $e' = 0.026$ (the minimum value reached by the eccentricity of Jupiter), the two domains of chaoticity separate (or almost separate) from each other as shown in Figure 13. Figure 13b which is a detail of Figure 13 is composed of five different trajectories. To the left a chaotic trajectory associated with the secondary resonance $\omega_p = 0$ (integrated for 10^7

years). In the middle a group of three trajectories integrated for 2.10^6 years, two of them are chains of islands and the middle on shows a slight chaoticity. This pattern is one of a set of *cantori* just after dissolution and a slightly smaller value of e' should show there a set of regular orbits. To the right of the diagram, a chaotic orbit associated with the crossing of the separatrix of the model problem (integrated for 10^7 years).

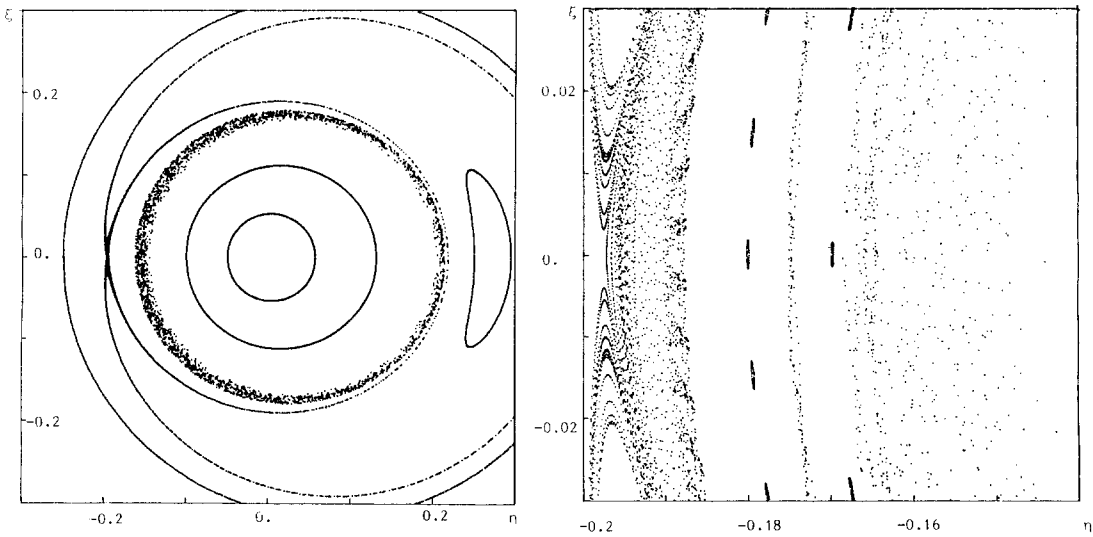

Fig. 13. Numerically integrated surface of section (ψ=0 , H=-2.10^{-5}) with e' =0.026 . Figure 13b is a detail of Figure 13a and is commented in the text.

From this example, we can appreciate that indeed the chaotic sea associated with the separatrix of the model problem covers a larger area than the Chirikov's stochastic layer of the secondary resonance. Nevertheless the last one does exist as a separate entity and furthermore it is from a qualitative point of view the important one. Indeed it is the one that shows the random jumps between a *high eccentricity mode* and a *low eccentricity mode* that were so puzzling when first discovered by Wisdom but were later explained (Wisdom 1985). The other chaotic layer (the slow Hamiltonian chaotic layer) remains in the low eccentricity mode.

7. Conclusions

In the line of Wisdom's perturbative technique for the 3/1 Jovian resonance (Wisdom 1985), Henrard and Lemaître (1986) have described a semi-numerical approach for the 2/1 Jovian resonance. This semi-numerical approach when applied to the problem considered by Wisdom (the averaged truncated planar elliptic problem) is not equivalent to the original perturbative technique of Wisdom.

In this paper we have improved a technical point of Henrard and Lemaître semi-numerical approach and compared it with the results of the original perturbative technique of Wisdom and with results obtained by numerical integration. The

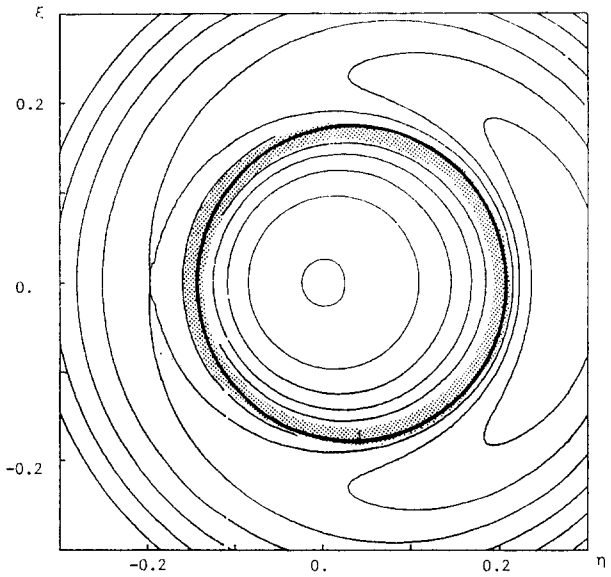

Fig. 14. Theoretical surface of section corresponding to Figure 13.

comparison is in general satisfactory even though we have identified a weak point of the method (see in Section 4 the comment after (36)).

The fact that the semi-numerical approach reproduces the main features described by Wisdom for the truncated (at order 2 in eccentricities) elliptic problem at the 3/1 Jovian resonance, is an indication that it is worth applying to other resonances or to more refined model of the 3/1 resonance as we plan to do in the near future.

Our comparison of the two methods and the description of our results may also be of interest by pointing out some aspects of the problem which were not emphasized in Wisdom's treatment. The role of secondary resonances is the most important of these aspects. In other resonance problems or as we have indicated in the same problem but with a smaller value of the eccentricity of the perturbing body its role may be prominent.

References

Borderies, N., and Goldreich, P. : 1984, "A simple derivation of capture probabilities", *Celest. Mech.*, **32**, 127-136.

Escande, D.F. : 1985, "Change of adiabatic invariant at separatrix crossing : Application to slow Hamiltonian chaos". In "*Advances in Nonlinear Dynamics and Stochastic Processes*" (R. Livi and A. Politi eds.), World Scientific, Singapore, 67-69.

Froeschlé, C., and Scholl, H. : 1976, "On the dynamical topology of the Kirkwood gaps", *Astron. Astrophys.*, **48**, 389-393.

Froeschlé, C., and Scholl, H. : 1977, "A qualitative comparison between the circular and elliptic Sun-Jupiter-Asteroid problem at commesurabilities", *Astron. Astrophys.*, **57**, 33-39.

Froeschlé, C., and Scholl, H. : 1981, "The stochasticity of peculiar orbits in the 2/1 Kirkwood gap", *Astron. Astrophys.*, **93**, 62-66.

Giffen, R. : 1973, "A study of commensurable motion in the asteroid belt", *Astron. Astrophys.*, **23**, 387-403.
Henrard, J. : 1988, "Resonances in the Planar Elliptic Restricted Problem". In *Long Term Behaviour of Natural and Artificial N-Body Systems*, (A. Roy ed.).
Henrard, J. : 1989, "The adiabatic invariant in Classical Mechanics", *Dynamics Reported*, to be published.
Henrard, J., and Lemaître, A. : 1986, "A perturbation method for problems with two critical arguments", *Celest. Mech.*, **39**, 213-238.
Henrard, J., and Lemaître, A. : 1987, "A perturbative treatment of the 2/1 Jovian resonance", *Icarus*, **69**, 266-279.
Henrard, J., Lemaître, A., Milani, A. and Murray, C.D. : 1986, "The reducing transformation and apocentric librators", *Celest. Mech.*, **38**, 335-344.
Koiller, J., Balthazar, J.M. and Yokoyama, T. : 1987, "Relaxation-chaos phenomena in Celestial Mechanics", *Physica*, **26D**, 85-122.
Lemaître, A. : 1984, "High order resonance in the restricted three body problem", *Celest. Mech.*, **32**, 109-126.
Lemaître, A., and Henrard, J. : 1989, "Chaotic motion in the 2/1 resonance", *Icarus* in print.
Message, J.P. : 1966, "On nearly commensurable periods in the restricted problem of three bodies", *Proc. I.A.U. Symp. No. 25*, 197-222.
Murray, C.D. : 1986, "Structure of the 2/1 and 3/2 Jovian resonances", *Icarus*, **65**, 70-82.
Murray, C.D., and Fox, K. : 1984, "Structure of the 3/2 Jovian resonance : A comparison of numerical methods", *Icarus*, **59**, 221-233.
Peale, S.J. : 1986, "Orbital resonance, unusual configurations and exotic rotation states", in *Satellites* (J. Burns and M. Matthews eds.), Univ. of Arizona Press, 159-223.
Poincaré, H. : 1899, *Les méthodes nouvelles de la Mécanique Céleste*, Gauthier Villars (Tome II, p. 43).
Poincaré, H. : 1902, "Sur les planètes du type d'Hécube", *Bull. Astron.*, **19**, 289-310.
Scholl, H., and Froeschlé, C. : 1974, "Asteroidal motion at the 3/1 commensurability", *Astron. Astrophys.*, **33**, 455-458.
Scholl, H., and Froeschlé, C. : 1975, "Asteroidal motion at the 5/2, 7/3 and 2/1 resonances", *Astron. Astrophys.*,**42**, 457-463.
Schubart, J. : 1966, "Special cases of the restricted problem of three bodies", *Proc. of the I.A.U. Symp. No. 25*, 187-193.
Sessin, W., and Ferraz-Mello, S. : 1984, "Motion of two planets with period commensurable in the ratio 2/1", *Celest. Mech.*, **32**, 307-332.
Szebehely, V. : 1967, *Theory of Orbits*, Academic Press.
Wisdom, J. : 1982, "The origin of the Kirkwood's gaps : A mapping for asteroidal motion near the 3/1 commensurability", *Astron. J.*,**85**, 1122-1133.
Wisdom, J. : 1983, "Chaotic behaviour and the origin of the 3/1 Kirkwood gap", *Icarus*, **56**, 51-74.
Wisdom, J. : 1985, "A perturbative treatment of motion near the 3/1 commensurability", *Icarus*, **63**, 272-289.
Wisdom, J. : 1986, "Canonical solution of the two critical argument problem", *Celest. Mech.*,**38**, 175-180.
Wisdom, J. : 1987, "Urey prize lecture : Chaotic dynamics in the Solar System", *Icarus*, **72**, 241-275.